National direct-drive program on OMEGA and the National Ignition Facility

2017 Plasma Phys. Control. Fusion 59 014008

(http://iopscience.iop.org/0741-3335/59/1/014008)

IOP Publishing Plasma Physics and Controlled Fusion

Plasma Phys. Control. Fusion **59** (2017) 014008 (7pp) doi:10.1088/0741-3335/59/1/014008

National direct-drive program on OMEGA and the National Ignition Facility

V N Goncharov[1,2], S P Regan[1], E M Campbell[1], T C Sangster[1], P B Radha[1], J F Myatt[1,2], D H Froula[1,3], R Betti[1,2,3], T R Boehly[1], J A Delettrez[1], D H Edgell[1], R Epstein[1], C J Forrest[1], V Yu Glebov[1], D R Harding[1], S X Hu[1], I V Igumenshchev[1], F J Marshall[1], R L McCrory[1,2,3], D T Michel[1], W Seka[1], A Shvydky[1], C Stoeckl[1], W Theobald[1,2] and M Gatu-Johnson[4]

[1] Laboratory for Laser Energetics, University of Rochester, Rochester, NY 14623, USA
[2] Department of Mechanical Engineering, University of Rochester, Rochester, NY 14623, USA
[3] Department of Physics and Astronomy, University of Rochester, Rochester, NY 14623, USA
[4] Massachusetts Institute of Technology, Plasma Science and Fusion Center, Cambridge, MA 02139, USA

E-mail: vgon@lle.rochester.edu

Received 1 July 2016, revised 16 August 2016
Accepted for publication 25 August 2016
Published 18 October 2016

Abstract

A major advantage of the laser direct-drive (DD) approach to ignition is the increased fraction of laser drive energy coupled to the hot spot and relaxed hot-spot requirements for the peak pressure and convergence ratios relative to the indirect-drive approach at equivalent laser energy. With the goal of a successful ignition demonstration using DD, the recently established national strategy has several elements and involves multiple national and international institutions. These elements include the experimental demonstration on OMEGA cryogenic implosions of hot-spot conditions relevant for ignition at MJ-scale energies available at the National Ignition Facility (NIF) and developing an understanding of laser-plasma interactions and laser coupling using DD experiments on the NIF. DD designs require reaching central stagnation pressures in excess of 100 Gbar. The current experiments on OMEGA have achieved inferred peak pressures of 56 Gbar (Regan *et al* 2016 *Phys. Rev. Lett.* **117** 025001). Extensive analysis of the cryogenic target experiments and two- and three-dimensional simulations suggest that power balance, target offset, and target quality are the main limiting factors in target performance. In addition, cross-beam energy transfer (CBET) has been identified as the main mechanism reducing laser coupling. Reaching the goal of demonstrating hydrodynamic equivalence on OMEGA includes improving laser power balance, target position, and target quality at shot time. CBET must also be significantly reduced and several strategies have been identified to address this issue.

Keywords: ICF, hydroinstability, direct drive, cryogenic implosions, ignition

(Some figures may appear in colour only in the online journal)

1. Introduction

The main approach to ignition by means of laser-driven inertial confinement fusion (ICF) [1] currently pursued by the National Ignition Facility (NIF) [2] is x-ray (or indirect) drive (ID), where the laser energy absorbed in a high-Z hohlraum is re-emitted in the form of x rays that drive the fuel capsule. In the other mainline ICF laser approach, direct drive (DD), the target is driven by laser irradiation directly coupled to the plasma ablated from the imploding capsule. The main advantage of ID is reduced sensitivity of implosions to short-scale beam nonuniformities. The main advantage of DD is higher coupling efficiency (by a factor of 3–5) of the laser energy into kinetic energy of the shell (hydrodynamic efficiency) compared to that of ID. The OMEGA Laser System [3] and the KrF laser NIKE at the Naval Research Laboratory (NRL)

[4] have been the principal facilities for DD experiments in the United States. When the decision of pursuing ID as the main ICF approach was made by the U.S. ICF program back in 1976, single-beam laser quality was a major concern for achieving high compression in DD implosions, without the shell breaking apart from the Rayleigh–Taylor (RT) instability [1] seeded by laser imprint. Early challenges in improving beam uniformity have been resolved over the last several decades by introducing several beam-smoothing techniques. These include distributed phase plates (DPP's) [5], polarization smoothing with birefringent wedges [6], and smoothing by spectral dispersion (SSD) [7]. In addition, implementing adiabat-shaping techniques [8, 9] significantly reduced the impact of RT instability growth during shell acceleration. Also, imprint reduction was demonstrated by using mid-*Z*-doped ablators [10] and high-*Z* target overcoats [11]. Such progress and the challenges in achieving ignition on the NIF using ID [12] suggest considering direct drive as a viable alternative for developing a burning-plasma platform in a laboratory. In addition to the conventional 'hot-spot' ignition designs, several alternative direct-drive ignition schemes have been proposed in the past. Shock ignition [13], the most promising approach, is currently being considered as an alternative symmetric direct-drive ignition design for the NIF.

Compared to x-ray drive, direct-drive targets couple a larger fraction of laser energy into shell kinetic energy and internal energy of the neutron-producing central region of the target (hot spot) at peak fuel compression. This relaxes the requirement on shell convergence and hot-spot pressure in an igniting target. The ignition condition follows from Lawson criterion [14, 15], which can be written in a form commonly used in the ICF community as [1]

$$(\rho R)_{\rm hs} \times T \gtrsim 0.3\ {\rm g\ cm^{-2}} \times 5\ {\rm keV}, \qquad (1)$$

where ρ, $R_{\rm hs}$, and T are the hot-spot density, radius, and ion temperature, respectively. The requirement shown in equation (1) is intuitively simple: the hot-spot temperature must be around 5 keV for PdV work of the incoming shell to overcome radiation losses and have an alpha-particle production rate sufficient to create bootstrap heating; the areal density of $\sim$0.3 g cm^{-2} is required to stop alpha particles inside the hot spot at these temperatures. A product of these two quantities enters into the ignition condition since ignition at lower temperatures and higher areal densities is still possible because the cold shell becomes more opaque to radiation at higher shell areal densities (assuming that larger hot-spot areal density lead to larger shell areal densities), limiting radiation losses from the hot spot [15]. Substituting expressions for the pressure $p_{\rm hs} = (1+Z)\rho T/m_{\rm i}$ (Z is the average ion charge and $m_{\rm i}$ is the average ion mass) and internal energy $E_{\rm hs} = 3/2\ p_{\rm hs} V_{\rm hs}$ ($V_{\rm hs}$ is the neutron-averaged hot-spot volume) into equation (1) gives a minimum pressure requirement (threshold) for ignition,

$$p_{\rm hs} > p_{\rm thr} \equiv 250\ {\rm Gbar}\left(\frac{E_{\rm hs}}{10\ {\rm kJ}}\right)^{-1/2},\ {\rm or}\ \bar{P} \equiv \frac{p_{\rm hs}}{p_{\rm thr}}$$
$$= \left(\frac{p_{\rm hs}}{250\ {\rm Gbar}}\right)\sqrt{\frac{E_{\rm hs}}{10\ {\rm kJ}}} > 1, \qquad (2)$$

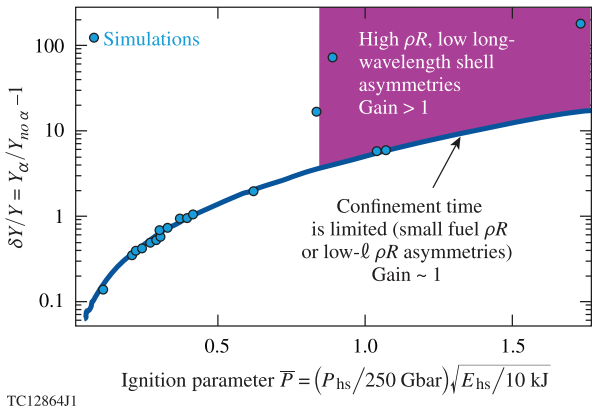

Figure 1. Alpha-amplification factor $\delta Y/Y$ as function of the ignition pressure parameter $\bar{P}$. The points represent the results of 1D *LILAC* simulations of designs at different laser energies in the range of OMEGA to NIF scale. The solid line shows a fit to the simulation results at $\bar{P} < 1$, $\delta Y/Y = \bar{P}e^{1.7\bar{P}^{2/3}}$

where $\bar{P}$ is the ignition pressure parameter. Equation (2) also sets the limit on the hot-spot volume in an igniting target:

$$V_{\rm hs} < V_{40}\left(\frac{E_{\rm hs}}{10\ {\rm kJ}}\right)^{3/2},\ {\rm or}\ \max(R_{\rm hs}) \sim \sqrt{E_{\rm hs}}, \qquad (3)$$

where $V_{40} = 4\pi/3(40\ \mu{\rm m})^3$ is the volume of a 40 μm sphere. Figure 1 plots the alpha-amplification factor ($Y_\alpha/Y_{{\rm no}-\alpha} - 1$, where Y_α and $Y_{{\rm no}-\alpha}$ are the target yields with and without alpha-particle deposition and fuel heating, respectively) as function of ignition pressure parameter $\bar{P}$. The plot is obtained using 1D *LILAC* [16] simulations of cryogenic targets at different laser drive energies (from OMEGA- to the NIF-scale designs). The solid line in the figure shows a fit to the simulation results at $\bar{P} < 1$, $\delta Y/Y = \bar{P}\exp(1.7\bar{P}^{2/3})$. $\bar{P} \sim 1$ defines the ignition threshold. When $\bar{P} > 1$ and the fuel areal density at peak compression is large enough ($(\rho R)_{\rm fuel} > 1$ g cm^{-2}) to burn a significant fraction of the main fuel, the target gain greatly exceeds unity ($G > 10$). In simulations where the main fuel areal density is low, the shell burnup fraction is not significant and the yield amplification continues to follow the fit even for $\bar{P} > 1$.

Spherically symmetric direct-drive cryogenic designs on OMEGA presently couple up to 0.44 kJ (out of 26 kJ incident laser energy) into the hot-spot internal energy [17]. When hydrodynamically scaled to the NIF-size laser energy (1.5 MJ to 1.8 MJ), these designs are predicted to couple 5× to 10× more energy into the hot spot (25 kJ–40 kJ for DD designs, depending on the laser coupling efficiency) compared to that of ID (4 kJ–5 kJ is inferred in the current best-performing ID implosions on the NIF), resulting in 2.5× to 3× lower hot-spot pressures required for DD ignition. The hot-spot size also gets larger with $E_{\rm hs}$ (see equation (3)), leading to smaller shell convergence (Cr $\sim$ 22 compared to 35–40 in ID ignition designs) and resulting in less-demanding long-wavelength drive-uniformity requirements.

With the goal of a successful ignition demonstration using direct drive, the recently established national DD strategy has several elements and involves multiple facilities and institutions, including the OMEGA laser as a leading facility for

DD research, NRL (which leads the effort on laser imprint reduction and has a major role in mitigation of coupling losses caused by laser-plasma interaction (LPI)), Lawrence Livermore National Laboratory (which recently established a DD working group concentrating its effort on understanding LPI at ignition-relevant scales, developing DD target designs with yields in the range from 100 kJ to a few MJ, and developing 3D computational capability for DD applications), Los Alamos National Laboratory (which leads the effort in simulating high-Z overcoats, experimental study of long-wavelength drive asymmetry, and developing platforms to study material properties in the warm-dense-matter regime). The elements of DD strategy include the experimental demonstration on OMEGA the hot-spot conditions ($p_{\rm hs} > 100$ Gbar) relevant for ignition at MJ-scale laser energies available on the NIF and developing an understanding of LPI and laser coupling using DD experiments on the NIF in the current indirect-drive configuration.

2. OMEGA cryogenic implosions

The target performance depends on both the drive and uniformity conditions. We begin this section with a discussion on the 1D physics.

2.1. 1D physics

To emphasize the importance of drive conditions in ignition target designing, the 1D scaling laws (which exclude multi-dimensional effects) for peak pressure and hot-spot energy are written in terms of implosion parameters: implosion velocity $v_{\rm imp}$ (the peak mass-averaged shell velocity), the peak drive (ablation) pressure p_a, adiabat of the unablated fuel mass α (ratio of the shell pressure to Fermi pressure at shell density), and peak in shell kinetic energy $E_{\rm kin}$ [18]:

$$p_{\rm hs}^{\rm 1D} \sim \frac{p_a^{1/3} {v_{\rm imp}}^{10/3}}{\alpha},\ E_{\rm hs}^{\rm 1D} \sim E_{\rm kin}\frac{{v_{\rm imp}}^{4/3}}{\alpha^{2/5} p_a^{4/15}},$$
$$\bar{P}_{\rm 1D} \sim \frac{\sqrt{E_{\rm kin}}\,{v_{\rm imp}}^4 p_a^{1/5}}{\alpha^{6/5}}. \qquad (4)$$

Modeling these critical implosion parameters must be experimentally validated before an assessment of the importance of multi-dimensional effects on the target performance can be made. The implosion velocity and shell kinetic energy are inferred in an experiment by measuring ablation-front trajectory and mass ablation rate using self-emission imaging [19]. The ablation pressure is inferred from simulations that match the measured ablation-front trajectory, mass ablation rate, bang time [20], and scattered-light power and spectrum [18, 21]. Finally, the shock-induced adiabat is inferred by measuring shock velocities early in the pulse using VISAR [22]. An additional increase in the fuel adiabat caused by hot-electron preheat is estimated by measuring the hard x-ray signal [23] and areal density [24, 25] in mid- to high-adiabat implosions (the areal density in 1D, for a given laser energy, depends mainly on shell adiabat [26], $\rho R \sim \alpha^{-0.5}$). A detailed comparison of 1D simulation results using *LILAC* with the data shows good agreement between the two for a variety of target designs and drive conditions [18]. One-dimensional simulations include nonlocal thermal transport model [27], a ray-based cross beam energy transfer (CBET) model [28] (see discussion on CBET in section 2.5), and first-principle EOS (FPEOS) models [29] for both the DT ice and CD ablator.

2.2. Multidimensional effects

The stability properties of indirect- and direct-drive designs are different. In direct drive, a thin CH layer is ablated from the shell early in the pulse to take advantage of the higher hydrodynamic efficiency of DT [18]. Since the shell consists mainly of DT during acceleration, the fuel adiabat α (which enters into the ignition scaling laws shown in equation (4)) and the average inflight shell adiabat $\alpha_{\rm shell}$ (which determines shell stability property) are approximately equal, $\alpha \sim \alpha_{\rm shell}$ ($\alpha_{\rm shell} \gtrsim \alpha$ in adiabat-shaped designs [9]). Then, the shell inflight aspect ratio (IFAR, defined as ratio of the target radius to the shell thickness) can be written as [30]

$$\mathrm{IFAR_{D.D}} \sim {v_{\rm imp}}^2/(p_a^{2/5}\alpha_{\rm shell}^{3/5}) \sim {v_{\rm imp}}^2/(p_a^{2/5}\alpha^{3/5}). \qquad (5)$$

While the inflight shell adiabat in DD designs is determined primarily by the strength of initial shocks (the radiation preheat in DD cryogenic implosions raises the fuel adiabat by ~20%), the shell adiabat and IFAR in ID designs is determined mainly by the radiation transport, ablator opacity, and x-ray drive spectrum (the majority of shell mass during acceleration in indirect drive consists of the ablator material; ablator and main fuel masses become approximately equal at the end of acceleration). As a result,

$$\mathrm{IFAR_{I.D}} \propto {v_{\rm imp}}^2/(p_a^{2/5}\alpha^{3/5}). \qquad (6)$$

Note that even though IFAR and the ablation-front RT growth in ID are determine by the x-ray heating of the ablator and not by the strength of initial shocks, the initial condition for RT instability is set during the shock propagation through the shell early in the drive, so-called the Richtmyer–Meshkov (RM) phase of perturbation evolution [31]. Therefore, the difference in the stability properties of indirectly driven shells for $\alpha = 1.4$ and 'high-foot' $\alpha = 2.5$ designs [12] are caused mainly by differences in nonuniformity growth during the RM phase [32].

Substituting equation (5) into equation (4) gives the hot-spot scaling laws for DD implosions:

$$p_{\rm hs}^{\rm 1D} \sim p_a \mathrm{IFAR}^{5/3},\ {V_{\rm hs}}^{\rm 1D} \sim \frac{E_{\rm kin}}{p_a \mathrm{IFAR}},\ E_{\rm hs}^{\rm 1D} \sim E_{\rm kin}\mathrm{IFAR}^{2/3},$$
$$\bar{P}_{\rm 1D} \sim p_a\sqrt{E_{\rm kin}}\,\mathrm{IFAR}^2. \qquad (7)$$

Equation (7) shows that the hot-spot pressure and the ignition pressure parameter $\bar{P}$ can be increased in 1D mainly by raising the shell IFAR (by reducing the shell mass, for example) and by making the laser drive more efficient (by increasing the ablation pressure and shell kinetic energy). The maximum value of IFAR in a design is set by the target stability properties and

the level of nonunifomity seeds: the short-scale modes (which satisfy $k\Delta < 1$, where k is the perturbation wave number and Δ is the inflight shell thickness) disrupt the shell during the implosion if IFAR is too large {current cryogenic implosions on OMEGA are unstable if IFAR$> 20(\alpha/3)^{1.1}$ [18]}. The long-wavelength perturbations ($k\Delta > 1$) seeded by the laser power imbalance, laser mispointing, and target misalignment can prevent the hot spot from reaching the 1D stagnation pressures if RT and Bell–Plesset (BP) [1] nonuniformity growth is excessively large during deceleration. The design IFAR can be increased, nevertheless, if the short-scale nonuniformities seeded by target imperfections and imprint are reduced, and the source the long-wavelength perturbations (beam imbalance, target offset, and beam mispointing) is minimized.

2.3. Target performance

Figure 2 shows the scaled ignition pressure parameter $\bar{P}$ inferred in OMEGA cryogenic implosions. Since $v_{\rm imp}$, p_a, and α are invariants with respect to laser energy $E_{\rm L}$, and $E_{\rm kin}$ is proportional to $E_{\rm L}$ (assuming constant laser coupling efficiency for different $E_{\rm L}$), $\bar{P}$ scales as $\sqrt{E_{\rm kin}}$ (see equation (2)). Thus, extrapolating the OMEGA results to the NIF-scale laser energy leads to $\bar{P}_{\rm scaled} = \bar{P}_{\rm OMEGA}(E_{\rm L}^{\rm NIF}/E_{\rm L}^{\rm OMEGA})^{1/2}$. The latter quantity is plotted in figure 2 for OMEGA cryogenic implosions driven at different values of the fuel adiabat (calculated using *LILAC* simulations). The hot-spot pressure and internal energy are inferred [17, 33] by using the measured neutron yield, burn duration $\Delta t_{\rm burn}$ [20], the neutron-average ion temperature $\langle T_{\rm i}\rangle_{\rm n}$, and hot-spot size. The experimentally inferred $\bar{P}_{\rm scaled}$ is shown with diamonds and the 1D *LILAC* predictions are shown with squares. The trend lines represent the best linear fit to the simulation data. The highest hot-spot pressure inferred in these experiments is 56 ± 7 Gbar [17]. According to figure 2, when scaled to the laser energy available on the NIF, the current OMEGA implosions reach up to ~40% of the pressure required for ignition. Then, using the alpha amplification scaling shown in figure 1, these implosions would yield a $2\times$ yield amplification due to alpha heating. Similar conclusions were reached using an independent calculation recently performed based on the $P\tau$ analysis [34].

To understand the trends shown in figure 2, the effects of shell nonuniformity must be considered. As the shell adiabat increases, the target performance becomes less sensitive to the nonuniformity growth, and the inferred $\bar{P}$ approaches the 1D-predicted values. For lower values of shell adiabat, on the other hand, the deviation of the observed $\bar{P}$ from the predictions increases. Since the 1D value of $\bar{P}$ decreases with the adiabat (see equation (4)), the inferred value has a maximum at $\alpha \sim 3.5$, which is a consequence of the interplay between a 1D reduction in $\bar{P}$ and a shell stability improvement as the adiabat increases.

The performance-degradation mechanisms in cryogenic DD implosions include both the short-scale growth (which breaks up the shell during acceleration and introduces mix between the ablator and the hot spot as well as between the cold, denser part of the fuel and the hot spot) and the long-wavelength modes. The latter increases the volume of a central, lower-density region (which forms the hot spot when the effects of asymmetry growth are negligible, but might contain colder regions excluded from the hot spot in a perturbed implosion) as well as create thin spots in the cold shell during deceleration, producing expanding bubbles that reduce pusher efficiency and limit hot-spot confinement [17, 35].

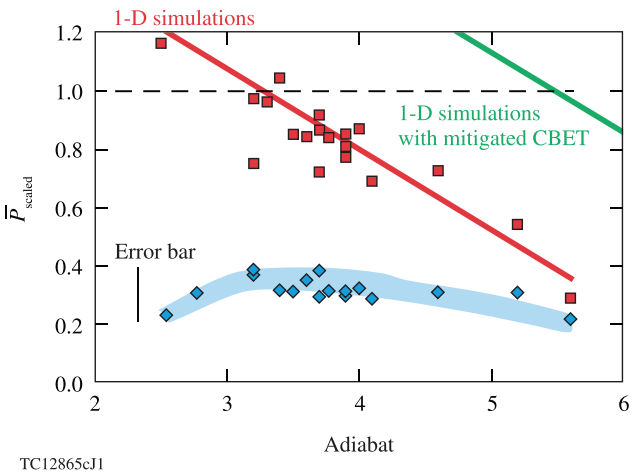

Figure 2. Ignition pressure parameter scaled to 1.8 MJ laser energy. Diamonds represent values inferred from the experimental data, squares show the 1D simulation results with full CBET effect, and the solid line marked by '1D simulation with mitigated CBET' represents a linear fit through simulations with CBET fully mitigated. The vertical line marked by 'error bar' shows a typical error bar for the inferred values of $\bar{P}$.

2.4. 3D simulation results

The evolution of long-wavelength nonuniformities seeded by the target offset, beam geometry, beam-power imbalance, and mispointing is studied using the 3D hydrocode *ASTER* [35]. These simulations show that such nonuniformities form bubbles (regions of low-density material that protrude from the central region into the higher-density shell) developed because of the deceleration RT and BP growth. As the shell continues to converge, the bubbles eventually break out of the shell, prematurely quenching the hot-spot confinement and neutron yield [33, 35]. Because nonuniformities cause the peak burn to occur earlier, the observations based on the fusion products sample the implosion conditions when the shell convergence has not reached yet the peak value. This effect and non-radial flows caused by the 3D effects prevent the fuel reaching stagnation, limiting conversion efficiency of shell kinetic energy into internal energy of the hot spot at peak burn.

The experimental evidence of low-mode asymmetries includes the x-ray self-emission imaging from a tracer Ti layer embedded into CH shell [36]. This technique shows significant low-mode nonuniformities developed during deceleration. Another self-emission imaging technique that maps the implosion shape during the acceleration indicates growth of low-l modes while the target is being driven by laser illumination [37]. In addition, significant variations in the measured

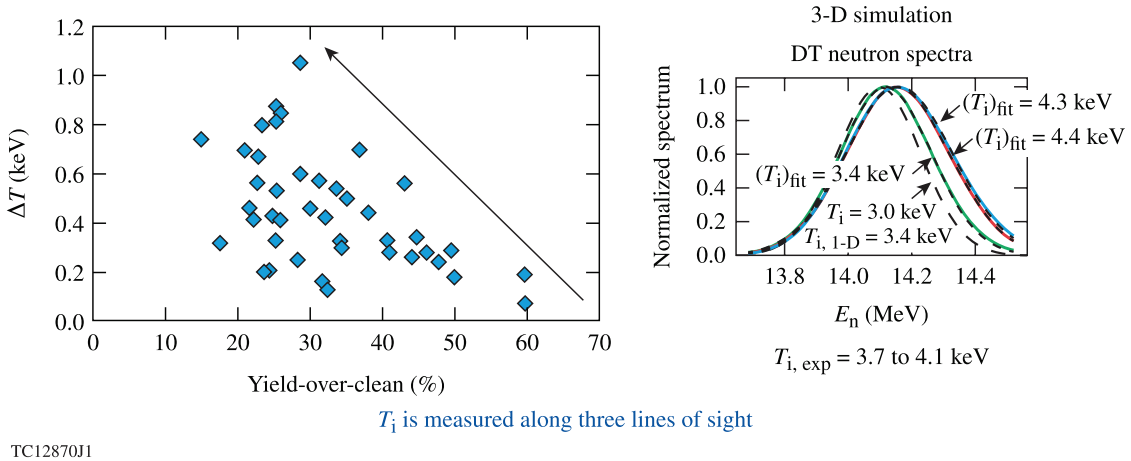

Figure 3. (left) The measured variation in ion temperature ΔT(keV) between three LOS in cryogenic implosions on OMEGA as function of yield-over-predictions. (right) Neutron spectra along three perpendicular views (solid lines) as calculated using ASTER simulations of an OMEGA cryogenic implosion assuming ~20 μm target offset and 15%-rms power imbalance. The dashed line shows the neutron spectrum without the effects of the bulk fuel motion.

ion temperature along different lines of sight (LOS) in cryogenic implosions are also indicative of asymmetry flows. The ion temperature is inferred in an experiment by measuring the spectral width of neutrons created as a result of fusing D and T. The spectral broadening, however, is caused not only by the thermal effects but also by the bulk motion with velocity distribution not aligned in a single direction. This results in higher temperature inferred from the fit $\langle T\rangle_{\rm fit}$ compared to the true thermal ion temperature T [30, 38]: $\langle T\rangle_{\rm fit} \simeq T + 2/3 m_i V_f^2$, where m_i is the average mass of fusion-reaction products and V_f is the bulk velocity. Since asymmetry growth creates different V_f along different LOS, different values of ion temperature are inferred along multiple LOS in a highly distorted implosion. The maximum measured temperature difference along three LOS's in OMEGA cryogenic implosions is shown in figure 3. The inferred temperature differences, up to 1 keV, correspond to non-radial flow velocities of $V_f \sim 2.5 \times 10^7$ cm s^{-1}. This is consistent with the results of 3D ASTER simulations which include the effect of power imbalance and target offset. The plot on the right in figure 3 shows the calculated neutron spectra at three perpendicular views (solid lines) together with neutron spectrum calculated without the effect of bulk motion (dashed line). Figure 3 also shows that the measured temperature variation strongly correlates with the yield degradation relative to the 1D predictions, suggesting that the residual kinetic energy plays a detrimental role in reducing the target performance.

The performance degradation in lower-adiabat implosions ($\alpha < 2.5$) are caused by both the long wavelengths (as described above) and the short-scale nonuniformities. The latter are seeded mainly by laser imprint, nonuniformities caused by target fabrication, and debris accumulated during cryogenic target production. Simulations indicate that the surface defects are the most damaging since they quickly evolve into nonlinear bubbles (modulations that produce local depressions in shell density) at the ablation front which are not stabilized by ablation [39] and grow at a rate exceeding the classical limit. Such growth leads to the ablator mixing into the main fuel and the vapor region [40]. These effects are directly observed in experiments. The ablator-cold shell mix is inferred from the backlit images obtained using monochromatic x-ray imager [41]. The observed enhancement in x-ray attenuation by the main fuel in low-adiabat implosion, not predicted by 1D calculations, is consistent with 0.1% to 0.2% atomic mixing of C into DT. No mixing is required to explain the observed fuel opacity in higher-adiabat implosions ($\alpha > 3.5$). In addition, the x-ray core emission at peak compression is also enhanced when the fuel adiabat is reduced to $\alpha < 2.5$, indicating that ablator carbon penetrates all the way into the hot spot during the implosion [42]. The plastic ablator in direct drive designs is thin and gets ablated in the middle of the drive pulse. Presence of the ablator in the hot spot suggests therefore a significant growth of the local surface features which produce jet-like structures in the shell early in the implosion and bring the ablator material into the hot spot [40].

2.5. Laser coupling and CBET

The shell stability properties can be significantly improved by increasing laser coupling and making the shell thicker. This can be accomplished by increasing the drive hydroefficiency. The analysis of direct-drive implosions on OMEGA has shown that coupling losses related to CBET [28] significantly limit the ablation pressure (as much as 40% on OMEGA and up to 60% on NIF-scale targets), implosion velocity, and shell kinetic energy. CBET results from scattering of the incoming laser light caused by stimulated Brillouin scatter. The reduction in the ablation pressure caused by CBET is shown in figure 4, where the ablation pressure, calculated at the time when the ablation surface has converged by a factor of 2.5, is plotted for OMEGA and NIF-scale symmetric designs at different drive intensities. Considering such losses, demonstrating the hydrodynamic equivalence of implosions on OMEGA to ignition designs on the NIF requires the shell IFAR to exceed the current stability threshold level (~22) [18].

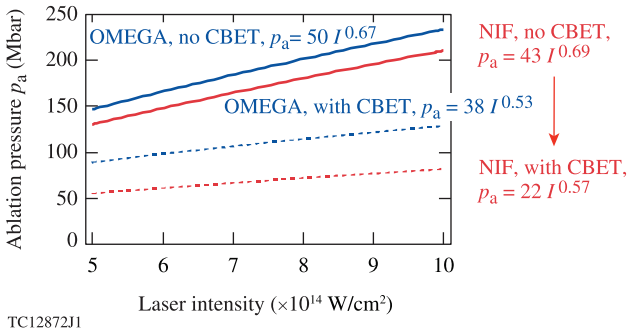

Figure 4. Ablation pressure as function of incident laser intensity for OMEGA and NIF-scale designs. Solid lines show calculation results without the effect of CBET and the dashed line are with this effect. The ablation pressure is calculated when the ablation front has converged by a factor of 2.5 from its initial radius. The shown pressure scaling is in Mbar and the laser intensity is in 10^{14} W cm^{-2}.

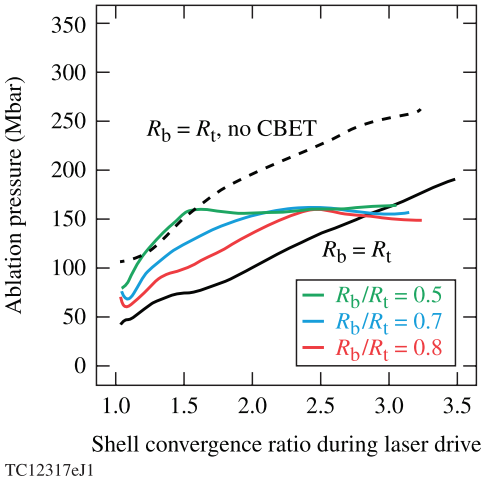

Figure 5. Time-dependent ablation pressure as function of shell convergence for designs driven at $I = 9 \times 10^{14}$ W cm^{-2}.

One of the CBET mitigation strategies [43] involves reducing the laser beam size relative to the initial target size. This strategy, as demonstrated both theoretically and experimentally, recovers some coupling losses and increases the ablation pressure [28, 33, 44]. The benefit of reducing beam size to enhance laser coupling is illustrated in figure 5 where the predicted time-dependent ablation pressure (plotted as function of shell convergence) is shown for different ratios of R_b/R_{target} (R_b is defined as the radius of a 95% beam-energy contour). Figure 5 shows that the largest increase in coupling occurs early in the implosion when the critical surface is at larger radius and the refraction effects prevent beams intersecting in regions where CBET is effective (Mach ~1 surface in plasma corona). Later in the implosion when the critical surface has moved inward a sufficient distance, beams start to intersect in the CBET-resonant regions and exchange their energy, increasing CBET losses. When CBET is fully mitigated, the shell kinetic and hot-spot internal energy increase, allowing implosions to the reach ignition condition at higher adiabat. This is illustrated in figure 2 where the trend line labeled as '1D simulations with mitigated CBET' shows the ignition pressure parameter with the enhanced laser coupling. The adiabat in the ignition designs can be increased in this case up to $\alpha \sim 5.5$, significantly improving shell stability properties.

Experimental campaigns performed on OMEGA with the reduced R_b/R_{target} have demonstrated increased hydrodynamic efficiency [33]. The target performance in such implosions, however, was degraded. This was explained, based on the results of 3D *ASTER* simulations [35], by asymmetries caused by power imbalance, enhanced in these implosions because of reduced beam overlap.

3. Conclusions

The direct-drive approach to ignition offers a significant increase (by a factor of 3–5) in laser coupling to the shell kinetic energy compared to indirect-drive designs. Cryogenic implosions on OMEGA have reached the hot-spot pressures of 56 Gbar, which is ~40% of what is required for ignition. Extrapolating these results to NIF-scale laser energy is predicted to enhance the yield due to alpha heating by a factor of 2. The cryogenic campaigns with reduced beam size relative to the target size ($R_b/R_{target} < 1$), performed on OMEGA to reduce CBET losses, demonstrated increased laser coupling and hydrodynamic efficiency. This coupling enhancement, however, did not improve the target performance. Numerical simulations indicate that long-wavelength nonuniformities caused by target offset and power imbalance lead to an increased target central volume and early burn truncation. Reaching the goal of demonstrating hydrodynamic equivalence on OMEGA includes improving laser power balance, target position, and target quality at shot time. CBET must also be reduced to increase the fuel mass and improve shell stability. CBET mitigation strategies include reduction in the beam size relative to the target size and laser wavelength separation [45].

Acknowledgments

This material is based upon work supported by the Department of Energy National Nuclear Security Administration under Award Number DE-NA0001944, the University of Rochester, and the New York State Energy Research and Development Authority. The support of DOE does not constitute an endorsement by DOE of the views expressed in this article. This report was prepared as an account of work sponsored by an agency of the U.S. Government. Neither the U.S. Government nor any agency thereof, nor any of their employees, makes any warranty, express or implied, or assumes any legal liability or responsibility for the accuracy, completeness, or usefulness of any information, apparatus, product, or process disclosed, or represents that its use would not infringe privately owned rights. Reference herein to any specific commercial product, process, or service by trade name, trademark, manufacturer, or otherwise does not necessarily constitute or imply its endorsement, recommendation, or favoring by the U.S. Government or any agency thereof. The views and opinions of authors

expressed herein do not necessarily state or reflect those of the U.S. Government or any agency thereof.

References

[1] Atzeni S and Meyer-ter-Vehn J 2004 *The Physics of Inertial Fusion: Beam Plasma Interaction, Hydrodynamics, Hot Dense Matter* (*Int. Series of Monographs on Physics*) (Oxford: Clarendon)
[2] Paisner J, Boyes J D, Kumpan S A, Lowdermilk W H and Sorem M S 1994 *Laser Focus World* **30** 75
[3] Boehly T R *et al* 1997 *Opt. Commun.* **133** 495
[4] Obenschain S P *et al* 1996 *Phys. Plasmas* **3** 2098
[5] Kessler T J, Lin Y, Armstrong J J and Velazquez B 1993 *Laser Coherence Control: Technology and Applications* vol 1870, ed H T Powell and T J Kessler (Bellingham, WA: SPIE) p 95
[6] Boehly T R, Smalyuk V A, Meyerhofer D D, Knauer J P, Bradley D K, Craxton R S, Guardalben M J, Skupsky S and Kessler T J 1999 *J. Appl. Phys.* **85** 3444
[7] Skupsky S, Short R W, Kessler T, Craxton R S, Letzring S and Soures J M 1989 *J. Appl. Phys.* **66** 3456
[8] Goncharov V N, Knauer J P, McKenty P W, Radha P B, Sangster T C, Skupsky S, Betti R, McCrory R L and Meyerhofer D D 2003 *Phys. Plasmas* **10** 1906
[9] Goncharov V N *et al* 2010 *Phys. Rev. Lett.* **104** 165001
[10] Hu S X, Fiksel G, Goncharov V N, Skupsky S, Meyerhofer D D and Smalyuk V A 2012 *Phys. Rev. Lett.* **108** 195003
[11] Obenschain S P *et al* 2002 *Phys. Plasmas* **9** 2234
[12] Hurricane O A *et al* 2014 *Nature* **506** 7488
[13] Betti R, Zhou C D, Anderson K S, Perkins L J, Theobald W and Solodov A A 2007 *Phys. Rev. Lett.* **98** 155001
[14] Lawson J D 1957 *Proc. Phys. Soc. Lond.* B **70** 6
[15] Betti R, Chang P Y, Spears B K, Anderson K S, Edwards J, Fatenejad M, Lindl J D, McCrory R L, Nora R and Shvarts D 2010 *Phys. Plasmas* **17** 058102
[16] Delettrez J, Epstein R, Richardson M C, Jaanimagi P A and Henke B L 1987 *Phys. Rev.* A **36** 3926
[17] Regan S P *et al* 2016 *Phys. Rev. Lett.* **117** 025001
[18] Goncharov V N *et al* 2014 *Phys. Plasmas* **21** 056315
[19] Michel D T, Sorce C, Epstein R, Whiting N, Igumenshchev I V, Jungquist R and Froula D H 2012 *Rev. Sci. Instrum.* **83** 10E530
[20] Stoeckl C, Glebov V Yu, Roberts S, Sangster T C, Lerche R A, Griffith R L and Sorce C 2003 *Rev. Sci. Instrum.* **74** 1713
[21] Seka W *et al* 2008 *Phys. Plasmas* **15** 056312
[22] Barker L M and Hollenbach R E 1972 *J. Appl. Phys.* **43** 4669
[23] Stoeckl C, Glebov V Yu, Meyerhofer D D, Seka W, Yaakobi B, Town R P J and Zuegel J D 2001 *Rev. Sci. Instrum.* **72** 1197
[24] Frenje J A, Li C K, Séguin F H, Casey D T, Petrasso R D, Sangster T C, Betti R, Glebov V Yu and Meyerhofer D D 2009 *Phys. Plasmas* **16** 042704
[25] Forrest C J *et al* 2012 *Rev. Sci. Instrum.* **83** 10D919
[26] Betti R and Zhou C 2005 *Phys. Plasmas* **12** 110702
[27] Goncharov V N *et al* 2008 *Phys. Plasmas* **15** 056310
[28] Igumenshchev I V, Edgell D H, Goncharov V N, Delettrez J A, Maximov A V, Myatt J F, Seka W, Shvydky A, Skupsky S and Stoeckl C 2010 *Phys. Plasmas* **17** 122708
[29] Hu S X, Militzer B, Goncharov V N and Skupsky S 2010 *Phys. Rev. Lett.* **104** 235003
Hu S X, Collins L A, Goncharov V N, Kress J D, McCrory R L and Skupsky S 2015 *Phys. Rev.* E **92** 043104
[30] Goncharov V N 2013 *Laser-Plasma Interactions and Applications* (*Scottish Graduate Series*) ed P McKenna *et al* (New York: Springer) pp 135–83
[31] Goncharov V N *et al* 2006 *Phys. Plasmas* **13** 012702
[32] Clark D S *et al* 2014 *Phys. Plasmas* **21** 112705
[33] Goncharov V N *et al* 2016 *J. Phys.: Conf. Ser.* **717** 012008
[34] Bose A *et al* 2016 *Phys. Rev.* E **94** 011201
[35] Igumenshchev I V *et al* 2016 *Phys. Plasmas* **23** 052702
[36] Shah R C *et al* 2016 Systematic fuel cavity asymmetries in directly driven ICF implosions *Phys. Rev. Lett* submitted
[37] Michel D T *et al* 2015 *High Power Laser Sci. Eng.* **3** e19
[38] Murphy T J 2014 *Phys. Plasmas* **21** 072701
[39] Betti R and Sanz J 2006 *Phys. Rev. Lett* **97** 205002
[40] Igumenshchev I V, Goncharov V N, Shmayda W T, Harding D R, Sangster T C and Meyerhofer D D 2013 *Phys. Plasmas* **20** 082703
[41] Stoeckl C *et al* 2014 *Rev. Sci. Instrum.* **85** 11E501
[42] Sangster T C *et al* 2013 *Phys. Plasmas* **20** 056317
[43] Igumenshchev I V *et al* 2013 *Phys. Rev. Lett.* **110** 145001
[44] Froula D H *et al* 2013 *Phys. Plasmas* **20** 082704
[45] Igumenshchev I V *et al* 2012 *Phys. Plasmas* **19** 056314